

---

# SVD Contextual Sparsity Predictors for Fast LLM Inference

---

Georgii Serbin<sup>1</sup> Kirill Koshkin<sup>2</sup> Zhongao Sun<sup>1</sup> Anastasiya Bistrigova<sup>1,2</sup> C.C. Korikov<sup>1</sup>

## Abstract

Contextual sparsity is one of the approaches used to reduce computational complexity in the inference process of large language models (LLMs). Existing techniques for efficient LLM inference acceleration based on contextual sparsity with minimal accuracy degradation require training sparse pattern predictors. This paper presents a framework for accelerating inference of ReGLU-based feed-forward networks (FFNs) within LLMs. The proposed framework provides a fast, training-free method for building sparse pattern predictors using truncation-aware singular value decomposition (SVD) of the gate projection matrix, along with a threshold calibration algorithm, and inference executors supporting conditional computation on CUDA and CANN devices. Experiments on three sparse LLMs with an average activation sparsity level of 90% in the FFNs demonstrate up to a 1.8× reduction in end-to-end decoding time while maintaining less than 1% degradation in benchmark scores on tasks involving complex math and code generation. This work advances the deployment of LLMs on edge devices.

## 1. Introduction

The remarkable capabilities of LLMs have led to their widespread integration across diverse domains (Brown et al., 2020; Dong et al., 2024b). While on-device AI deployment offers advantages in privacy, latency, and cost compared to server-based solutions (Shankar, 2024), the substantial computational requirements of LLM inference present significant challenges for edge deployment.

A key characteristic of ReGLU-based LLMs is dynamic (or contextual) sparsity – the phenomenon where only a small subset of neurons within FFN blocks are activated for any given input. This inherent property enables inference

acceleration by reducing both computational overhead and memory bandwidth requirements during generation (Liu et al., 2023).

A prevalent approach for leveraging contextual sparsity involves employing lightweight, learnable sparsity predictors (Liu et al., 2023). These predictors generate input-specific sparse activation patterns prior to FFN forward passes. The sparse pattern identifies neuron indices that will produce positive dot products with the input vector. In ReGLU FFNs, computations for the remaining neurons can be safely skipped without affecting output correctness, as the activation function nullifies negative values. Nevertheless, prediction errors may arise from false negative classifications, which compromise model accuracy. Effective predictors must balance high recall rates with substantial sparsity ratios while maintaining sufficient speed to reduce end-to-end (E2E) text generation latency.

In this study, we present a simple yet effective technique leveraging low-rank singular value decomposition (SVD) to predict sparse patterns, thereby enabling significant inference acceleration in ReGLU-based LLMs. Our methodology employs low-rank approximations of gate projection weight matrices in each layer as lightweight predictors of the FFN block sparsity mask during generation. Unlike existing contextual sparsity prediction methods, our approach provides theoretical guarantees regarding prediction accuracy.

To enhance the accuracy of SVD-based predictors, we employ a combination of techniques:

- **Calibrated bias.** Direct application of SVD approximations as predictors results in notable accuracy degradation. However, we observe that SVD predictors exhibit strong separation capabilities. Introducing neuron-specific thresholds – implemented as bias terms – effectively mitigates this issue. These biases are calibrated offline using a custom greedy algorithm that does not require gradient computation.
- **Data whitening technique.** Given the predictor speed constraints, the rank must be significantly smaller than the hidden dimension. To improve prediction accuracy under these conditions, we apply truncation-aware data whitening (Wang et al., 2025a;b; Yuan et al., 2025).

<sup>1</sup>Huawei Technologies Ltd. <sup>2</sup>Moscow State University, Russia. Correspondence to: C.C. Korikov <constantine.korikov@gmail.com>.

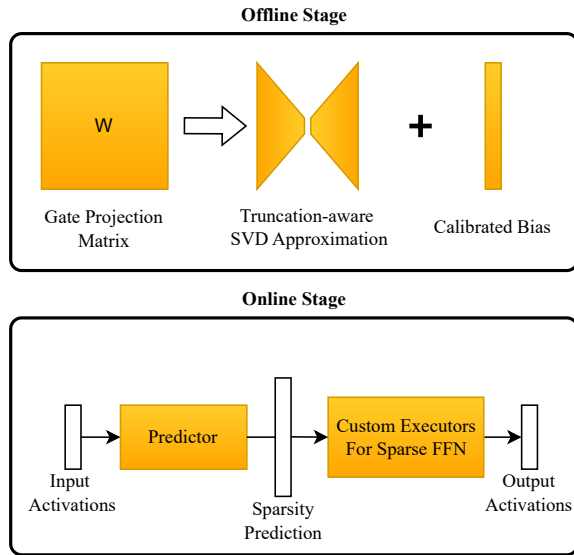


Figure 1. Overview of our framework. During the offline stage, sparsity predictors are constructed using low-rank SVD approximation with calibrated per-neuron thresholds. At inference time, SVD-based predictors precede each FFN block to exploit contextual sparsity and accelerate generation.

This technique reduces Frobenius norm error by incorporating input activation statistics, requiring only a small calibration dataset.

Implementation-level optimizations further enhance inference speedup:

- **Sequential computation of gate and up projections.** Gate and up projections are computed sequentially, enabling further acceleration through early elimination of false positive predictions. After computing gate projections, falsely activated neurons are identified and excluded from subsequent up and down projections, thereby increasing sparsity levels in the final FFN stages.
- **Inference executors.** Our implementations support conditional computation on CUDA (NVIDIA Corporation, 2024) and CANN (Huawei Technologies Co., Ltd., b) devices. For CUDA, we employ custom kernels rather than Triton-based abstractions (Tillet et al., 2019), prioritizing enhanced low-level control. On Huawei Ascend hardware (Liao et al., 2019), comparable performance gains are achieved exclusively through high-level PyTorch APIs, demonstrating effective utilization of the platform’s native software stack.

Figure 1 illustrates our framework architecture. Our key contributions are summarized as follows:

1. We propose training-free SVD-based contextual sparsity predictors for ReGLU-based LLM inference acceleration;
2. We introduce calibrated bias terms that significantly improve prediction accuracy, with biases tuned on small datasets using a custom gradient-free algorithm;
3. We develop executors supporting sparse FFN inference on CUDA and CANN devices;
4. We achieve up to  $1.8\times$  end-to-end inference speedup with minimal accuracy degradation.

## 2. Related Work

Sparsification is one of the most effective paradigms for accelerating LLM inference, typically categorized into **static** and **dynamic sparsity** methods.

**Static sparsity** removes redundant parameters before deployment (Ashkboos et al., 2024), reducing computation and memory costs but often sacrificing accuracy at high sparsity levels. In contrast, **dynamic sparsity** – also known as dynamic pruning or contextual sparsity – adapts sparsity patterns at runtime based on input context, enabling flexible efficiency-accuracy trade-offs.

**Predictor-based dynamic sparsity** methods, such as Deja Vu (Liu et al., 2023) and ShadowLLM (Akhaouri et al., 2024), learn lightweight neural predictors to estimate layer-wise sparsity. ShadowLLM enhances this approach by incorporating gradient information during training and utilizing a single predictor for all layers.

**Training-free dynamic sparsity** eliminates learned predictors and instead derives sparsity from activation statistics or calibrated thresholds. GRIFFIN (Dong et al., 2024a) selects active “expert” neurons using prefill activations, while TDA (Ma et al., 2024) introduces offline-calibrated thresholds allowing adaptive activation per layer. Both maintain fixed sparsity patterns within a prompt. CLADA (Yang et al., 2025) updates sparsity during generation but requires re-computation of previous states, hindering KV-cache reuse. TEAL (Liu et al., 2024) exploits input sparsity, which differs from activation sparsity in that it arises from redundancy in the input representations rather than neuron activations, using calibrated thresholds. SparseInfer (Shin et al., 2025) proposes a calibrated solution for ReLU-fied LLMs using sign-bit comparisons, which lacks theoretical justifications.

Dynamic sparsity can also underpin efficient on-device inference frameworks. PowerInfer (Song et al., 2024b) accelerates LLMs on consumer GPUs by preloading frequently activated neurons into GPU memory, minimizing CPU transfers. It achieves up to  $11.69\times$  speedup, particularly in CPU/GPU hybrid settings, whereas our work targets homogeneous

GPU inference with batch size one.

The effectiveness of dynamic sparsity depends heavily on activation functions. ReLU activations naturally induce sparse activations, unlike smoother functions such as Swish or SiLU used in modern LLMs (Zhang et al., 2024). Recent studies show that replacing them with ReLU variants plus fine-tuning recovers substantial sparsity (Mirzadeh et al., 2023). ProSparse (Song et al., 2024a) achieved  $\sim 90\%$  sparsity in LLaMA2-7B through progressive regularization and activation threshold shifting, while TurboSparse (Song et al., 2024c) used double ReLU (dReLU) activation function to sparsify models like Qwen2-7B and Mistral-7B.

Beyond pruning, SVD offers complementary compression capabilities. ASVD (Yuan et al., 2025) leverages activation-aware transformations to attain 10–30% model compression, and SVD-LLM (Wang et al., 2025b) provides theoretical connections between discarded components and  $L_2$  loss.

SparseLoRA (Khaki et al., 2025) integrates SVD-based estimators into parameter-efficient fine-tuning, dynamically slicing weights by input relevance. However, sparse computations are applied only to *context tokens* (the prefix tokens provided as input), while *output tokens* (the target tokens used for loss computation) remain densely processed to avoid performance degradation. Achieving accelerated and high-quality decoding of LLMs through contextual sparsity remains an open challenge not addressed by SparseLoRA.

### 3. Preliminaries

Consider a ReGLU-activated FFN block during decoding, defined as:

$$\text{FFN}(x) = W^{\text{down}} (\text{ReLU}(W^{\text{gate}}x) \odot (W^{\text{up}}x)), \quad (1)$$

where  $x \in \mathbb{R}^d$  is the input activation vector, and  $W^{\text{gate}}, W^{\text{up}} \in \mathbb{R}^{D \times d}$ , and  $W^{\text{down}} \in \mathbb{R}^{d \times D}$  are the gate, up-projection, and down-projection matrices, respectively. Here,  $d$  denotes the hidden size and  $D$  the intermediate size. Let  $X \in \mathbb{R}^{d \times N}$  denote the hidden states of  $N$  calibration tokens, and let  $r$  denote the predictor rank. For brevity, we omit layer indices.

Our objective is to obtain a predictor  $P$  that outputs a binary mask  $m = P(x) \in \{0, 1\}^D$  over the  $D$  intermediate neurons. This mask identifies active neurons by selecting the corresponding rows of  $W^{\text{gate}}$  and  $W^{\text{up}}$ , together with their aligned columns of  $W^{\text{down}}$ , yielding sparse computation algebraically equivalent to the dense FFN due to ReLU sparsity.

## 4. SVD-Based Sparsity Predictors

This section introduces *training-free SVD-based sparsity predictors* (SVDP), designed for efficient inference in

ReGLU-based LLMs. Our approach consists of two stages: an offline phase for predictor construction and an online phase for accelerated sparse inference.

### 4.1. Training-free Predictor Building

The predictors are constructed by approximating the gate projection matrix  $W^{\text{gate}}$  using a low-rank SVD decomposition. This approach offers a theoretical upper bound on local error (see Section A.1).

We propose predictors of the affine form

$$P(x) = H(ABx + b), \quad (2)$$

where  $H : \mathbb{R} \rightarrow \{0, 1\}$  is the Heaviside step function applied element-wise.  $H(z) = 1$  if  $z > 0$  and 0 otherwise. The product  $AB$  approximates  $W^{\text{gate}}$ , while  $b$  adjusts per-neuron decision thresholds.

#### 4.1.1. DATA-AWARE SVD-BASED FACTORIZATION

To improve the accuracy of the SVD approximation, we adopt a data whitening technique. This minimizes the Frobenius norm error:

$$\|WX - U_r \Sigma_r V_r^\top X\|_F \quad (3)$$

on calibration data  $X$ , by incorporating input statistics through a whitening matrix  $S$ :

$$\begin{aligned} W &= (WS)S^{-1} \\ &= (U\Sigma V^\top)S^{-1} \approx U_r \Sigma_r V_r^\top S^{-1} = AB. \end{aligned} \quad (4)$$

We follow Wang et al. (2025b) in choosing  $S$  as the Cholesky decomposition of  $XX^\top$ , which outperforms ASVD in terms of perplexity at low ranks, as shown in Table 2 of Yuan et al. (2025).

The predictor construction pipeline is described in Algorithm 1 and is performed independently for each layer. Throughout, we fix the predictor rank  $r$  across layers (see Section E.3 for a discussion on rank selection).

---

#### Algorithm 1 Building SVD-predictors (Offline Phase)

---

**Input:**  $W^{\text{gate}} \in \mathbb{R}^{D \times d}$ ,  $X \in \mathbb{R}^{d \times N}$ ,  $r \in \mathbb{N}$   
**Output:**  $A \in \mathbb{R}^{D \times r}$ ,  $B \in \mathbb{R}^{r \times d}$   
 $S \in \mathbb{R}^{d \times d} \leftarrow \text{Cholesky}(XX^\top)$   
 $U, \Sigma, V \leftarrow \text{SVD}(W^{\text{gate}}S)$   
 $A \in \mathbb{R}^{D \times r} \leftarrow U_{:,r} \Sigma_{:,r}$   
 $B \in \mathbb{R}^{r \times d} \leftarrow V_{:,r} S^{-1}$   
**return**  $A, B$

---

#### 4.1.2. THRESHOLD CALIBRATION

SVD-based sparsity predictors typically exhibit good separation between active and inactive neurons; however, naive

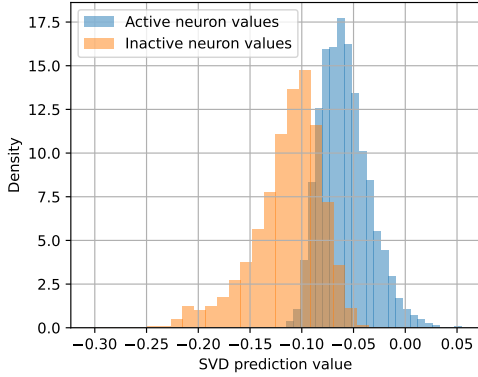


Figure 2. Distribution of SVD-based predictor outputs for a sample neuron. Although active and inactive states are well separated, zero thresholding causes significant false negatives for truly active neurons.

thresholding (e.g., at zero) leads to substantial accuracy degradation. This effect arises from a shift in the predictor output distribution induced by truncation of singular value components, as illustrated in Figure 2.

To compensate for this distribution shift, a bias term is introduced in the second layer of the SVD-based predictor. The central problem is to calibrate this bias so as to achieve a prescribed sparsity level while limiting the associated accuracy loss. Simple schemes that tune thresholds to match a target sparsity, recall, or accuracy on a calibration set were empirically found to yield suboptimal trade-offs.

Instead, a fast greedy calibration algorithm, Algorithm 2, is employed that explicitly accounts for the heterogeneous impact of different neurons on model accuracy. From a computational standpoint, all neurons are equally valuable for acceleration, since pruning any neuron reduces the cost by the same amount, whereas their contributions to output accuracy differ substantially. Consequently, some neurons require high recall, whereas others can tolerate higher false-negative rates without noticeably affecting overall performance. Under certain conditions, our greedy algorithm is guaranteed to provide an optimal solution (see Section A.2).

Let  $s \in (0, 1]$  denote the desired sparsity ratio, controlling the speed-accuracy trade-off (see Section E.3). For each neuron  $i \in [D]$ , initialize  $\tau_i \leftarrow \min_{t: w_i^{(t)} > 0} s_i^{(t)}$ . Then greedily increase sparsity by advancing the neuron with smallest incremental cost  $\sum_{j=1}^{\eta} w_{i, (k_i+j)}$  until

$$\frac{1}{DT} \sum_{i=1}^D \sum_{t=1}^T \mathbf{1}[s_i^{(t)} \leq \tau_i] \geq s.$$

The penalty  $C_i(k_i + \eta) - C_i(k_i)$  proxies FFN output perturbation across  $\eta$  samples. Fixed biases  $b = -\tau \in \mathbb{R}^D$  are

used during inference.

The proposed predictor is lightweight and data-efficient, requiring only few thousands of tokens for reliable construction and bias estimation. It is fast and memory-efficient, making it suitable for practical use in constrained settings.

## 4.2. Runtime Execution

We modify only the FFNs; the rest of the model remains unchanged. During inference, the prefill stage remains unchanged. At the decoding stage, we leverage CUDA and CANN executors for sparse FFN computation. Figure 3 illustrates the sparse inference pipeline, where speedup is determined by the token-dependent sparsity ratio.

**Sparsity Prediction** Our predictor comprises two linear layers, requiring no specialized implementation. DeJa Vu employs lookahead predictors to circumvent prediction latency. This is enabled via asynchronous computation, where predictor execution time is overlapped with data transfer from global memory or inter-process communication under tensor parallelism. However, such pipelining may be infeasible on certain hardware platforms (see Section B). Given our focus on local inference for edge deployment scenarios, similar to PowerInfer engine, our predictors are inserted at the beginning of each FFN and sequentially generate sparsity patterns for their respective gate projections.

**Gate/up Execution Order** A prevalent optimization for efficient deployment of LLMs with gated FFNs involves parallelized execution of the gate and up projections. While effective in dense computation scenarios, this approach presents non-trivial challenges for local inference systems leveraging sparse activations. We delineate two distinct computational methodologies to address this:

- *Parallel pipeline* e.g., PowerInfer. A predictor first generates a sparsity mask, which is concurrently applied to independently compute both gate and up projections. This maintains identical sparsity levels across both projections during execution.
- *Sequential pipeline* e.g., SparseInfer and our approach. The gate and up projections are computed sequentially, eliminating false positives: neurons predicted as active are revalidated after gate projection computation, further increasing sparsity in subsequent projections.

**Algorithmic Complexity** In our case, realized sparsity equals or exceeds the predicted sparsity  $s$  by filtering erroneous predictions. Thanks to sequential pipeline, we can use more lightweight predictors that provide relatively low sparsity at the gate projection stage without compromising the FFN’s performance.

**Algorithm 2** Greedy Bias Calibration (Offline Phase)

**Input:**

$W^{\text{gate}}, W^{\text{up}} \in \mathbb{R}^{D \times d}, W^{\text{down}} \in \mathbb{R}^{d \times D}$  – weight matrices,  
 $\mathcal{D} = \{x^{(t)} \in \mathbb{R}^d\}_{t=1}^T$  – calibration dataset,  
 $A, B$  – low-rank approximation from Algorithm 1,  
 $s \in [0; 1]$  – desired sparsity level,  $\eta$  – discrete step size.

**Output:**  $b \in \mathbb{R}^D$

$w_i^{(t)} \leftarrow |\text{ReLU}(W_{i,:}^{\text{gate}} x^{(t)}) \cdot W_{i,:}^{\text{up}} x^{(t)}|^2 \|W_{:,i}^{\text{down}}\|_2^2$  (Compute neurons' importance)

$s_i^{(t)} \leftarrow (ABx^{(t)})_i$  (Compute predictor's outputs)

**for**  $i = 1$  **to**  $D$  **do**

$s_{i,(1)} \leq \dots \leq s_{i,(T)}$  (Sort samples in nondecreasing order)

$C_i(k) = \begin{cases} \sum_{j=1}^k w_{i,(j)}, & k = 1, \dots, T \\ C_i(T), & T < k < T + \eta \\ +\infty, & k = T + \eta \end{cases}$  (Compute cumulative costs with padding)

$k_i \leftarrow \min\{k : w_{i,(k)} > 0\}, \tau_i \leftarrow s_{i,(k_i)}$  (Initialize pointers and thresholds)

**end for**

**while**  $\frac{1}{DT} \sum_{i=1}^D \sum_{t=1}^T \mathbf{1}[s_i^{(t)} \leq \tau_i] < s$  **do**

$i^* \leftarrow \arg \min_i [C_i(k_i + \eta) - C_i(k_i)]$  (Greedy step)

$k_{i^*} \leftarrow \max(k_{i^*} + \eta, T), \tau_{i^*} \leftarrow s_{i,(k_{i^*})}$  (Update pointers and thresholds)

**end while**

$b \leftarrow -\tau$

**return**  $b$

A dense FFN requires  $3dD$  multiplications (excluding element-wise product), whereas our sparse approach reduces this to:

$$\underbrace{r(d+D)}_{\text{predictor}} + \underbrace{d(1-s)D}_{\text{gate}} + \underbrace{2d(1-s')D}_{\text{up/down}} \quad (5)$$

where  $s$  is the predicted sparsity and  $s'$  the realized sparsity. For example, in ProSparse-LLaMA2-7B (Song et al., 2024a) ( $d = 4096, D = 11008, s = 0.5, s' = 0.9, r = 256$ ), operations decrease by  $3.8\times$ . Note that hardware-level dynamic sparsity challenges prevent this from directly translating to wall-clock speedup.

**Hardware platforms** CUDA and CANN devices are supported for sparse FFN inference. See implementation details in Section B.

## 5. Experimental Results

### 5.1. Experimental Setup

**Hardware** A single consumer-grade NVIDIA RTX 3090 GPU<sup>1</sup> at the MSU Laboratory of Computer Engineering

<sup>1</sup>All GPU-based experiments were conducted exclusively by authors affiliated with Moscow State University (Kirill Koshkin) without involvement of Huawei-affiliated researchers. Huawei-affiliated co-authors contributed solely to theoretical analysis, algorithm design and CANN performance evaluation.

is used for both quality and performance evaluation. The inference is performed entirely on GPU.

For evaluation on NPU, a single Ascend 310P3 (Huawei Technologies Co., Ltd., a) device is used.

**Software** We use the vLLM framework (Kwon et al., 2023), preferring it to the Transformers framework (Wolf et al., 2020) for the experiments, as it better reflects real-world deployment scenarios. Notably, we do not utilize any server-specific features of vLLM, such as tensor parallelism. Inference is performed in half precision, while predictor construction in the offline stage uses double precision.

**Models** We evaluate our solution across three open-source sparse 7B language models: **ProSparse-LLaMA2-7B** (Song et al., 2024a) and two instruction-tuned models – **SparseQwen2-7B** and **TurboSparse-Mistral-Instruct** (Song et al., 2024c).

The instruction-tuned models incorporate double ReLU (dReLU) activation in their FFN layers:

$$\text{FFN}(x) = W^{\text{down}}(\text{ReLU}(W^{\text{gate}}x) \odot \text{ReLU}(W^{\text{up}}x)) \quad (6)$$

**Quality Evaluation** We evaluate model performance using a diverse set of open-source benchmarks spanning reasoning, coding, knowledge, and multilingual understanding: **GSM8K** (Cobbe et al., 2021) (math reasoning), **HumanEval** (Chen et al., 2021) (code generation), **ARC-**

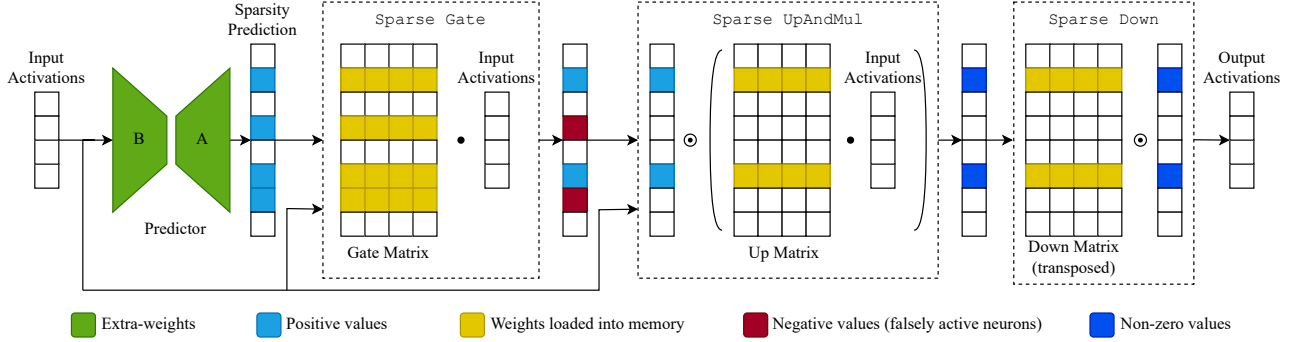


Figure 3. Sparse inference using SVD-based sparsity predictors. Neurons with positive predictor values are considered active during gate projection. Gate and up projections are executed sequentially to increase sparsity.

E/ARC-C (Clark et al., 2018) (scientific and common-sense reasoning), TriviaQA (Joshi et al., 2017) (open-domain QA), MBPP (Austin et al., 2021) (small Python tasks), BBH (Suzgun et al., 2022) (complex reasoning), and CMMLU (Li et al., 2024) (Chinese multi-task understanding).

We adopt the UltraEval framework (He et al., 2024), aligning with prior ProSparse evaluations, as the model shows compatibility issues with lm-eval-harness (Gao et al., 2024). All benchmarks use free-form generation rather than perplexity scoring to better reflect real-world LLM usage.

**Performance Evaluation** Model performance is measured using the PyTorch profiler (Ansel et al., 2024). For each domain, results are averaged across multiple samples. E2E latency includes the prefill stage and 200-token generation.

### 5.2. Performance Under Different Sparsity Ratios

The desired sparsity hyperparameter  $s$  from Algorithm 2 influences the calibrated thresholds and can be used to trade off accuracy and acceleration. As Table 1 shows, lower thresholds lead to lower sparsity and lower acceleration. In contrast, higher thresholds provide more speedup but may degrade quality. Long generation tasks are the most sensitive, while for short answer tasks the sparsity can be significantly increased. With our approach we can achieve up to  $1.8\times$  E2E generation speedup while maintaining less than 1% degradation in benchmark scores on tasks involving complex math and code generation. See Section D for detailed evaluation results.

### 5.3. Comparison With Other Methods

We compare SVDP against training-free sparsity methods (GRIFFIN (Dong et al., 2024a)) and learnable predictors (PowerInfer (Song et al., 2024b), Deja Vu (Liu et al., 2023)). GRIFFIN relies on prompt-based statistical sparsity patterns,

Table 1. Average accuracy when varying hyperparameter  $s$  for different models.  $s$  implicitly sets sparsity, which directly translates to end-to-end speedup.

Model	Method	$s$	Accuracy, %	Speedup
ProSparse-LLaMA2-7B	Dense	—	38.92	1.00 $\times$
	SVDP	0.4	38.66 (-0.26)	1.61 $\times$
		0.5	38.78 (-0.14)	1.64 $\times$
		0.6	38.77 (-0.15)	1.67 $\times$
		0.7	38.57 (-0.35)	1.71 $\times$
TurboSparse-Mistral-Instruct	Dense	—	54.30	1.00 $\times$
	SVDP	0.4	53.72 (-0.58)	1.67 $\times$
		0.5	53.56 (-0.74)	1.73 $\times$
		0.6	53.18 (-1.12)	1.79 $\times$
		0.7	53.44 (-0.86)	1.84 $\times$
SparseQwen2-7B	Dense	—	65.84	1.00 $\times$
	SVDP	0.4	65.41 (-0.43)	1.78 $\times$
		0.5	65.20 (-0.64)	1.81 $\times$
		0.6	65.13 (-0.71)	1.85 $\times$
		0.7	64.49 (-1.35)	1.86 $\times$

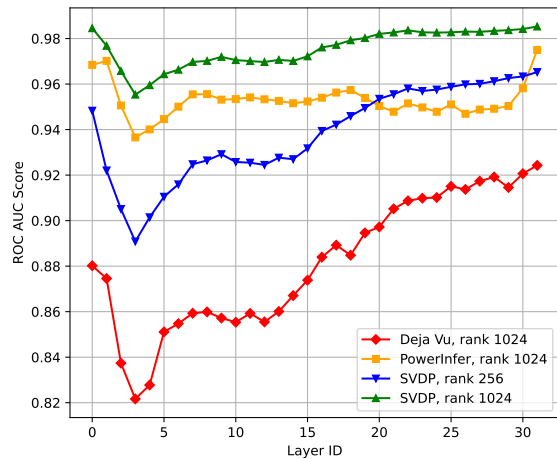


Figure 4. Layer-wise ROC AUC score of different predictors averaged across several sequence samples for ProSparse-LLaMA2-7B. AUROC score of 1 indicates perfect separation and AUROC score of 0.5 corresponds to random guessing.

## SVD Contextual Sparsity Predictors for Fast LLM Inference

Table 2. Comparison with other methods on ProSparse-LLaMA2-7B, evaluated in our framework ( $r = 1024$  parallel,  $r = 256$  sequential).

Method	Predicted sparsity, %	TriviaQA acc, %	ARC-E acc, %	ARC-C acc, %	HumanEval pass@1, %	MBPP pass@1, %	GSM8K acc, %	BBH acc, %	CMMLU acc, %	Average Score	E2E Speedup
Dense baseline	—	62.94	75.42	53.58	17.68	22.59	11.45	35.85	31.84	38.92	1.00×
<i>Trained predictors</i>											
Deja Vu	20	59.47	74.87	53.41	3.66	2.98	3.03	34.49	30.97	32.86	1.38×
PowerInfer	80	61.10	74.54	52.99	15.85	21.15	10.69	35.29	31.80	37.93	1.63×
<i>Training-free methods</i>											
GRIFFIN	20	59.77	74.75	53.33	15.85	22.18	8.95	35.49	32.01	37.79	1.14×
GRIFFIN	50	35.74	72.77	51.96	12.20	18.17	4.47	35.32	31.88	32.81	1.46×
<i>Ours</i>											
SVDP	75	62.66	75.38	53.58	17.68	22.18	10.54	35.86	31.85	38.72	1.61×
SVDP (seq.)	50	62.74	75.34	53.67	17.68	22.07	11.22	35.58	31.94	38.78	1.64×

while PowerInfer and Deja Vu use trained predictors.

For Deja Vu, we trained predictors following their official repository instructions. For PowerInfer, we used their recommended pretrained predictors.

**Benchmarks** Table 2 shows that our SVDP matches PowerInfer’s accuracy and sparsity while requiring less data and compute for construction. GRIFFIN struggles with stable performance at high sparsity ratios, particularly for long generations. The sequential pipeline implementation reduces SVDP size by 4× without compromising either accuracy or inference speed.

**ROC-AUC Analysis** We also evaluate predictor separation ability via layer-wise ROC-AUC scores on held-out test sequences (Figure 4). SVDP outperforms learnable baselines on unseen data. Trained predictors may suffer from out-of-distribution sensitivity due to their data-dependent nature, while SVD predictors directly leverage the LLM’s internal weight structure.

### 5.4. Ablation Study

Table 3 shows ablation of SVD sparsity estimators, starting from SparseLoRA’s baseline (Khaki et al., 2025) (referred to as Naive SVD):

- *Data whitening*: Incorporate input data statistics (Sec. 4.1.1).
- *Bias calibration*: Add neuron-specific bias terms (Sec. 4.1.2).

Bias calibration significantly improves accuracy by accounting for distribution shift after low-rank approximation.

Data whitening substantially enhances ROC-AUC separation vs. Naive SVD on held-out test sequences (Figure 5), independent of bias calibration.

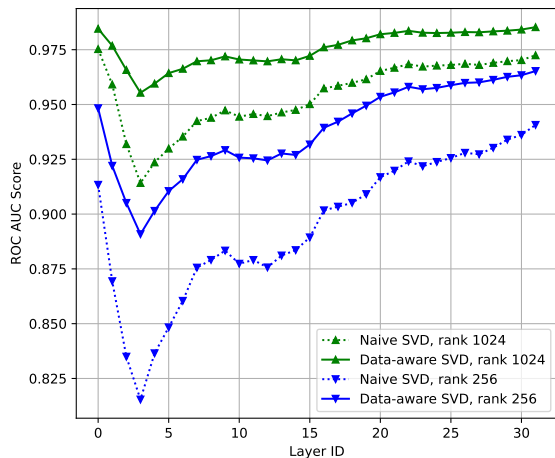


Figure 5. Layer-wise ROC-AUC: data-aware SVD vs. Naive SVD for ProSparse-LLaMA2-7B.

### 5.5. Inference Executors

Table 4 presents FFN performance of our CUDA and CANN executors across varying sparsity ratios. Here, we use Huawei’s Ascend 310P3 AI accelerator. Notably, we achieve comparable performance gains on the Ascend hardware using only high-level PyTorch APIs, eliminating the need for manual low-level instruction optimization. This result facilitates deeper exploration of contextual sparsity optimizations within the DaVinci architecture. It is worth noting that when the sparsity value approaches 90%, the L1 (Liao et al., 2019) cache hit rate reaches almost 100%, resulting in a significant speedup increase.

### 6. Limitations

- Our method targets sparse models where non-linear activation functions naturally produce significant zero-valued outputs. Extension to non-ReGLU-based architectures remains an important direction for future

Table 3. SVD sparsity estimator ablation study. †Averaged across all benchmarks (see Appendix D).

Configuration	ProSparseLLAMA2-7B			TurboSparse-Mistral-Instruct			SparseQwen2-7B		
	GSM8K	HumanEval	Average†	GSM8K	HumanEval	Average†	GSM8K	HumanEval	Average†
Dense baseline	11.45	17.68	38.92	61.71	34.15	54.30	77.1	64.02	65.84
<i>Parallel pipeline</i>									
Naive SVD	6.60	10.98	34.08	60.20	24.39	51.52	74.00	53.66	62.05
+ Data whitening	10.16	16.46	37.10	60.88	37.20	53.02	75.89	61.59	63.99
+ Bias calibration	10.54	17.68	38.72	62.24	36.59	54.34	76.65	62.20	65.37
<i>Sequential pipeline</i>									
Naive SVD	1.90	0.61	9.69	9.17	1.83	30.87	63.00	12.20	51.60
+ Data whitening	6.90	8.54	31.00	48.60	29.27	46.49	72.93	57.32	60.80
+ Bias calibration	11.22	17.68	38.78	61.41	33.54	53.56	76.80	62.80	65.22

Table 4. FFN performance of our CUDA and CANN executors at different sparsity ratios. The speedups are compared to the corresponding dense implementations. Predictors latency is not included. For this experiment, sparsity ratio is fixed across all linear layers.

LLM architecture	Sparsity, %	FFN Speedup	
		CUDA	CANN
ProSparseLLAMA2-7B	20	1.30×	0.76×
	50	1.90×	1.23×
	80	3.34×	3.38×
	95	4.67×	30.67×
TurboSparse-Mistral-Instruct	20	1.29×	0.76×
	50	1.90×	1.18×
	80	3.44×	3.10×
	95	4.92×	22.85×
SparseQwen2-7B	20	1.33×	0.81×
	50	1.95×	1.32×
	80	3.47×	3.41×
	95	4.91×	28.46×

research. See Section C for detailed discussion.

- Batched processing inherently reduces sparsity levels, limiting achievable speedups and precluding the use of sparsity predictors during the prefill phase.

## Conclusion

This paper introduces a training-free framework for accelerating the inference of ReGLU-based large language models through contextual sparsity exploitation. The proposed solution comprises two stages: (1) an offline calibration phase where sparsity predictors are constructed using data-aware truncated singular value decomposition of gate projection matrices with calibrated bias parameters, and (2) an online inference phase enabling efficient sparse LLM execution on CUDA and CANN devices. Evaluation across three sparse language models demonstrates up to  $1.8\times$  end-to-end decoding acceleration with minimal accuracy degradation across diverse benchmarks, including code and mathematical rea-

soning tasks.

## Acknowledgements

We thank the MSU Laboratory of Computer Engineering for conducting all GPU-based experiments. Huawei-affiliated authors declare no access to or involvement in GPU-based experiments due to U.S. export control regulations. No Huawei-affiliated researchers participated in GPU-dependent aspects of this work.

## Impact Statement

This paper presents an approach for accelerated inference of LLMs. While there are many potential societal consequences of our work, we do not believe any require specific highlighting here.

## References

- Akhauri, Y., AbouElhamayed, A. F., Dotzel, J., Zhang, Z., Rush, A. M., Huda, S., and Abdelfattah, M. S. Shad-owlm: Predictor-based contextual sparsity for large language models, 2024. URL <https://arxiv.org/abs/2406.16635>.
- Ansel, J., Yang, E., He, H., Gimelshein, N., Jain, A., Voznesensky, M., Bao, B., Bell, P., Berard, D., Burovski, E., Chauhan, G., Chourdia, A., Constable, W., Desmaison, A., DeVito, Z., Ellison, E., Feng, W., Gong, J., Gschwind, M., Hirsh, B., Huang, S., Kalambarkar, K., Kirsch, L., Lazos, M., Lezcano, M., Liang, Y., Liang, J., Lu, Y., Luk, C., Maher, B., Pan, Y., Puhersch, C., Reso, M., Saroufim, M., Siraichi, M. Y., Suk, H., Suo, M., Tillet, P., Wang, E., Wang, X., Wen, W., Zhang, S., Zhao, X., Zhou, K., Zou, R., Mathews, A., Chanan, G., Wu, P., and Chintala, S. PyTorch 2: Faster Machine Learning Through Dynamic Python Bytecode Transformation and Graph Compilation. In *29th ACM International Conference on Architectural Support for Programming Languages and Operat-*

- ing Systems, Volume 2 (ASPLOS '24)*. ACM, April 2024. doi: 10.1145/3620665.3640366. URL <https://docs.pytorch.org/assets/pytorch2-2.pdf>.
- Ashkboos, S., Croci, M., Gennari do Nascimento, M., Hoefler, T., and Hensman, J. Slicept: Compress large language models by deleting rows and columns. In Kim, B., Yue, Y., Chaudhuri, S., Fragkiadaki, K., Khan, M., and Sun, Y. (eds.), *International Conference on Representation Learning*, volume 2024, pp. 11682–11701, 2024.
- Austin, J., Odena, A., Nye, M., Bosma, M., Michalewski, H., Dohan, D., Jiang, E., Cai, C., Terry, M., Le, Q., and Sutton, C. Program synthesis with large language models, 2021. URL <https://arxiv.org/abs/2108.07732>.
- Brown, T. B., Mann, B., Ryder, N., Subbiah, M., Kaplan, J., Dhariwal, P., Neelakantan, A., Shyam, P., Sastry, G., Askell, A., Agarwal, S., Herbert-Voss, A., Krueger, G., Henighan, T., Child, R., Ramesh, A., Ziegler, D. M., Wu, J., Winter, C., Hesse, C., Chen, M., Sigler, E., Litwin, M., Gray, S., Chess, B., Clark, J., Berner, C., McCandlish, S., Radford, A., Sutskever, I., and Amodei, D. Language models are few-shot learners. In *Proceedings of the 34th International Conference on Neural Information Processing Systems, NIPS '20*, Red Hook, NY, USA, 2020. Curran Associates Inc. ISBN 9781713829546.
- Chen, M., Tworek, J., Jun, H., Yuan, Q., de Oliveira Pinto, H. P., Kaplan, J., Edwards, H., Burda, Y., Joseph, N., Brockman, G., Ray, A., Puri, R., Krueger, G., Petrov, M., Khlaaf, H., Sastry, G., Mishkin, P., Chan, B., Gray, S., Ryder, N., Pavlov, M., Power, A., Kaiser, L., Bavarian, M., Winter, C., Tillet, P., Such, F. P., Cummings, D., Plappert, M., Chantzis, F., Barnes, E., Herbert-Voss, A., Guss, W. H., Nichol, A., Paino, A., Tezak, N., Tang, J., Babuschkin, I., Balaji, S., Jain, S., Saunders, W., Hesse, C., Carr, A. N., Leike, J., Achiam, J., Misra, V., Morikawa, E., Radford, A., Knight, M., Brundage, M., Murati, M., Mayer, K., Welinder, P., McGrew, B., Amodei, D., McCandlish, S., Sutskever, I., and Zaremba, W. Evaluating large language models trained on code, 2021. URL <https://arxiv.org/abs/2107.03374>.
- Clark, P., Cowhey, I., Etzioni, O., Khot, T., Sabharwal, A., Schoenick, C., and Tafjord, O. Think you have solved question answering? try arc, the ai2 reasoning challenge, 2018. URL <https://arxiv.org/abs/1803.05457>.
- Cobbe, K., Kosaraju, V., Bavarian, M., Chen, M., Jun, H., Kaiser, L., Plappert, M., Tworek, J., Hilton, J., Nakano, R., Hesse, C., and Schulman, J. Training verifiers to solve math word problems, 2021. URL <https://arxiv.org/abs/2110.14168>.
- Dong, H., Chen, B., and Chi, Y. Prompt-prompted adaptive structured pruning for efficient LLM generation. In *First Conference on Language Modeling*, 2024a. URL <https://openreview.net/forum?id=4aqq9xTtih>.
- Dong, X., Zhang, X., Bu, W., Zhang, D., and Cao, F. A survey of llm-based agents: Theories, technologies, applications and suggestions. In *2024 3rd International Conference on Artificial Intelligence, Internet of Things and Cloud Computing Technology (AIoTC)*, pp. 407–413, 2024b. doi: 10.1109/AIoTC63215.2024.10748304.
- Gao, L., Tow, J., Abbasi, B., Biderman, S., Black, S., DiPofi, A., Foster, C., Golding, L., Hsu, J., Le Noac’h, A., Li, H., McDonell, K., Muennighoff, N., Ociepa, C., Phang, J., Reynolds, L., Schoelkopf, H., Skowron, A., Sutawika, L., Tang, E., Thite, A., Wang, B., Wang, K., and Zou, A. The language model evaluation harness, 07 2024. URL <https://zenodo.org/records/12608602>.
- He, C., Luo, R., Hu, S., Zhao, Y., Zhou, J., Wu, H., Zhang, J., Han, X., Liu, Z., and Sun, M. Ultraeval: A lightweight platform for flexible and comprehensive evaluation for llms, 2024.
- Huawei Technologies Co., Ltd. Atlas 200 AI Accelerator Module User Guide. <https://support.huawei.com/enterprise/en/doc/EDOC1100223189/968ec576/basic-specifications>, a. Official product page of the Ascend 310P3 chip.
- Huawei Technologies Co., Ltd. Ascend CANN. <https://www.hiascend.com/zh/cann>, b. Official product page of CANN for Ascend AI chip series.
- Joshi, M., Choi, E., Weld, D. S., and Zettlemoyer, L. Triviaqa: A large scale distantly supervised challenge dataset for reading comprehension, 2017. URL <https://arxiv.org/abs/1705.03551>.
- Khaki, S., Li, X., Guo, J., Zhu, L., Plataniotis, K. N., Yazdanbakhsh, A., Keutzer, K., Han, S., and Liu, Z. SparseloRA: Accelerating LLM fine-tuning with contextual sparsity. In *Forty-second International Conference on Machine Learning*, 2025. URL <https://openreview.net/forum?id=z83rodY0Pw>.
- Kwon, W., Li, Z., Zhuang, S., Sheng, Y., Zheng, L., Yu, C. H., Gonzalez, J. E., Zhang, H., and Stoica, I. Efficient memory management for large language model serving with pagedattention. In *Proceedings of the ACM SIGOPS 29th Symposium on Operating Systems Principles*, 2023.
- Li, H., Zhang, Y., Koto, F., Yang, Y., Zhao, H., Gong, Y., Duan, N., and Baldwin, T. Cmmlu: Measuring massive multitask language understanding in chinese, 2024. URL <https://arxiv.org/abs/2306.09212>.

- Liao, H., Tu, J., Xia, J., and Zhou, X. Davinci: A scalable architecture for neural network computing. In *2019 IEEE Hot Chips 31 Symposium (HCS)*, pp. 1–44, 2019. doi: 10.1109/HOTCHIPS.2019.8875654.
- Liu, J., Ponnusamy, P., Cai, T., Guo, H., Kim, Y., and Athiwaratkun, B. Training-free activation sparsity in large language models, 2024. URL <https://arxiv.org/abs/2408.14690>.
- Liu, Z., Wang, J., Dao, T., Zhou, T., Yuan, B., Song, Z., Shrivastava, A., Zhang, C., Tian, Y., Re, C., et al. Deja vu: Contextual sparsity for efficient llms at inference time. In *International Conference on Machine Learning*, pp. 22137–22176. PMLR, 2023.
- Ma, C., Huang, M., Zhang, Y., Wang, C., Wang, Y., Yu, L., Liu, C., and Lin, W. First activations matter: Training-free methods for dynamic activation in large language models, 2024. URL <https://arxiv.org/abs/2408.11393>.
- Mirzadeh, I., Alizadeh, K., Mehta, S., Mundo, C. C. D., Tuzel, O., Samei, G., Rastegari, M., and Farajtabar, M. Relu strikes back: Exploiting activation sparsity in large language models, 2023. URL <https://arxiv.org/abs/2310.04564>.
- NVIDIA Corporation. *CUDA C Programming Guide*, 12.4 edition, July 2024. URL <https://docs.nvidia.com/cuda/cuda-c-programming-guide/index.html>. Version 12.4 of the CUDA Toolkit.
- Shankar, V. Edge ai: A comprehensive survey of technologies, applications, and challenges. In *2024 1st International Conference on Advanced Computing and Emerging Technologies (ACET)*, pp. 1–6, 2024. doi: 10.1109/ACET61898.2024.10730112.
- Shin, J., Yang, H., and Yi, Y. Sparseinfer: Training-free prediction of activation sparsity for fast llm inference. In *2025 Design, Automation & Test in Europe Conference (DATE)*, pp. 1–7, 2025. doi: 10.23919/DATE64628.2025.10992997.
- Song, C., Han, X., Zhang, Z., Hu, S., Shi, X., Li, K., Chen, C., Liu, Z., Li, G., Yang, T., and Sun, M. ProSparse: Introducing and enhancing intrinsic activation sparsity within large language models. *arXiv preprint arXiv:2402.13516*, 2024a. URL <https://arxiv.org/pdf/2402.13516.pdf>.
- Song, Y., Mi, Z., Xie, H., and Chen, H. Powerinfer: Fast large language model serving with a consumer-grade gpu, 2024b. URL <https://arxiv.org/abs/2312.12456>.
- Song, Y., Xie, H., Zhang, Z., Wen, B., Ma, L., Mi, Z., and Chen, H. Turbo sparse: Achieving llm sota performance with minimal activated parameters, 2024c. URL <https://arxiv.org/abs/2406.05955>.
- Suzgun, M., Scales, N., Schärli, N., Gehrmann, S., Tay, Y., Chung, H. W., Chowdhery, A., Le, Q. V., Chi, E. H., Zhou, D., and Wei, J. Challenging big-bench tasks and whether chain-of-thought can solve them, 2022. URL <https://arxiv.org/abs/2210.09261>.
- Tillet, P., Kung, H. T., and Cox, D. Triton: an intermediate language and compiler for tiled neural network computations. In *Proceedings of the 3rd ACM SIGPLAN International Workshop on Machine Learning and Programming Languages*, MAPL 2019, pp. 10–19, New York, NY, USA, 2019. Association for Computing Machinery. ISBN 9781450367196. doi: 10.1145/3315508.3329973. URL <https://doi.org/10.1145/3315508.3329973>.
- Wang, X., Alam, S., Wan, Z., Shen, H., and Zhang, M. SVD-LLM v2: Optimizing singular value truncation for large language model compression. In Chiruzzo, L., Ritter, A., and Wang, L. (eds.), *Proceedings of the 2025 Conference of the Nations of the Americas Chapter of the Association for Computational Linguistics: Human Language Technologies (Volume 1: Long Papers)*, pp. 4287–4296, Albuquerque, New Mexico, April 2025a. Association for Computational Linguistics. ISBN 979-8-89176-189-6. doi: 10.18653/v1/2025.naacl-long.217. URL <https://aclanthology.org/2025.naacl-long.217/>.
- Wang, X., Zheng, Y., Wan, Z., and Zhang, M. SVD-LLM: Truncation-aware singular value decomposition for large language model compression. In *International Conference on Learning Representations (ICLR)*, 2025b. URL <https://openreview.net/forum?id=LNYIUouhdt>.
- Wolf, T., Debut, L., Sanh, V., Chaumond, J., Delangue, C., Moi, A., Cistac, P., Rault, T., Louf, R., Funtowicz, M., Davison, J., Shleifer, S., von Platen, P., Ma, C., Jernite, Y., Plu, J., Xu, C., Scao, T. L., Gugger, S., Drame, M., Lhoest, Q., and Rush, A. M. Transformers: State-of-the-art natural language processing. In *Proceedings of the 2020 Conference on Empirical Methods in Natural Language Processing: System Demonstrations*, pp. 38–45, Online, October 2020. Association for Computational Linguistics. URL <https://www.aclweb.org/anthology/2020.emnlp-demos.6>.
- Yang, Y., Wang, Y., Ma, C., Yu, L., Chersoni, E., and Huang, C.-R. Sparse brains are also adaptive brains: Cognitive-load-aware dynamic activation for llms, 2025. URL <https://arxiv.org/abs/2502.19078>.

Yuan, Z., Shang, Y., Song, Y., Yang, D., Wu, Q., Yan, Y., and Sun, G. Asvd: Activation-aware singular value decomposition for compressing large language models, 2025. URL <https://arxiv.org/abs/2312.05821>.

Zhang, Z., Song, Y., Yu, G., Han, X., Lin, Y., Xiao, C., Song, C., Liu, Z., Mi, Z., and Sun, M. Relu2 wins: Discovering efficient activation functions for sparse llms. *ArXiv*, abs/2402.03804, 2024. URL <https://api.semanticscholar.org/CorpusID:267499856>.

## A. Theoretical Analysis

### A.1. Predictor error bounds

Let  $m, d > 0$  and  $0 < r \leq \min(m, d)$ . Consider a weight matrix  $W \in \mathbb{R}^{m \times d}$  and its rank- $r$  approximation  $W_r \in \mathbb{R}^{m \times d}$  (e.g., truncated SVD), with bias vector  $b \in \mathbb{R}^m$ . For any input  $x \in \mathbb{R}^d$ ,  $x \neq 0$ , we have:

$$A(x) := \text{ReLU}(Wx), \quad (7)$$

$$g_b(x) := \mathbf{1}[W_r x + b > 0], \quad (8)$$

$$B_b(x) := A(x) \odot g_b(x). \quad (9)$$

Throughout, we use the following notation:

$$\delta_i \in \mathbb{R}^m, \quad i \in [m], \quad \text{denotes the } i\text{-th standard basis vector } (0, \dots, \underbrace{1}_i, \dots, 0)^\top,$$

$$t_+ := \max(t, 0), \quad \text{the ReLU function (i.e., } t_+ = 0 \text{ if } t < 0 \text{ and } t_+ = t \text{ if } t \geq 0).$$

We aim to derive deterministic bounds on the relative gating error

$$\mathcal{E}_b(x) := \frac{\|A(x) - B_b(x)\|_2}{\|x\|_2}$$

in terms of the spectral error of  $W_r$  and the bias  $b$ .

#### Exact error representation and monotonicity

**Definition A.1** (Residual operator). Define the residual matrix and residual vector

$$\Delta W := W - W_r, \quad e(x) := \Delta W x.$$

**Proposition A.2** (Exact representation of the gating error). *For every  $x \in \mathbb{R}^d$ ,*

$$A(x) - B_b(x) = \text{ReLU}(Wx) \odot \mathbf{1}[W_r x + b \leq 0], \quad (10)$$

and therefore

$$\|A(x) - B_b(x)\|_2^2 = \sum_{i=1}^m ((Wx)_i)_+^2 \mathbf{1}[(W_r x + b)_i \leq 0]. \quad (11)$$

*Proof.* The claim follows immediately from the componentwise definition of  $B_b(x)$ .  $\square$

**Proposition A.3** (Monotonicity w.r.t. biases). *Let  $b, b' \in \mathbb{R}^m$  and suppose  $b' \leq b$  componentwise. Then for all  $x \in \mathbb{R}^d$ ,*

$$\|A(x) - B_{b'}(x)\|_2 \geq \|A(x) - B_b(x)\|_2.$$

*Proof.* If  $b' \leq b$ , then  $\mathbf{1}[W_r x + b \leq 0] \leq \mathbf{1}[W_r x + b' \leq 0]$  componentwise. Using the identity (10) and the fact that  $\text{ReLU}(Wx) \geq 0$  componentwise, the  $\ell_2$  norm can only increase when we replace  $b$  by the smaller bias  $b'$ , which activates the mask on a superset of coordinates.  $\square$

*Remark A.4.* Using thresholds  $\tau = -b$  clarifies the trade-off: increasing  $\tau$  increases sparsity (more gates are off) but never decreases the error; equivalently, increasing  $b$  reduces sparsity and never increases the error.

**A deterministic bound via the shifted residual**

**Lemma A.5** (Residual-based upper bound). *For every  $x \in \mathbb{R}^d$  and  $b \in \mathbb{R}^m$ ,*

$$\|A(x) - B_b(x)\|_2 \leq \|(\Delta W x - b)_+\|_2 \leq \|\Delta W x - b\|_2. \quad (12)$$

*Proof.* Let  $z = Wx$ ,  $z_r = W_r x$ , and  $e := z - z_r = \Delta W x$ . Define the gated index set

$$I := \{i \in [m] : (z_r + b)_i \leq 0\}.$$

By definition,

$$\|A(x) - B_b(x)\|_2^2 = \sum_{i \in I} (z_i)_+^2.$$

For  $i \in I$  we have  $z_{r,i} \leq -b_i$ , hence  $z_i = z_{r,i} + e_i \leq e_i - b_i$ . By monotonicity of  $t \mapsto (t)_+$ ,  $(z_i)_+ \leq (e_i - b_i)_+$ . Therefore

$$\sum_{i \in I} (z_i)_+^2 \leq \sum_{i=1}^m (e_i - b_i)_+^2 = \|(e - b)_+\|_2^2,$$

which gives the first inequality. The second inequality follows from  $\|(u)_+\|_2 \leq \|u\|_2$ .  $\square$

**Worst-case bounds** Due to the previous result, the analysis of the nonlinear gating error reduces to a deterministic quantity depending only on the residual  $\Delta W x$  and the bias  $b$ . We therefore can study the worst-case value

$$\sup_{\|e\|_2 \leq R} \|(e - b)_+\|_2,$$

which characterizes the maximal gating error at residual energy  $R$ .

**Uniform bias**

**Theorem A.6** (Worst-case bound for uniform bias). *Let  $b = \beta \mathbf{1}$  with  $\beta \in \mathbb{R}$ . For all  $R \geq 0$ ,*

$$\sup_{\|e\|_2 \leq R} \|(e - \beta \mathbf{1})_+\|_2 = \begin{cases} (R - \beta)_+, & \beta \geq 0, \\ R - \beta\sqrt{m}, & \beta < 0. \end{cases}$$

*Proof.*

**Case 1:**  $\beta \geq 0$ . Write  $y := (e - \beta \mathbf{1})_+ \in \mathbb{R}_{\geq 0}^m$  and  $t := \|y\|_2$ .

Let  $S := \{i : y_i > 0\}$  (if  $t = 0$  there is nothing to prove, otherwise  $R > \beta$ ).

For  $i \in S$  we have  $e_i = \beta + y_i$ , hence

$$\|e\|_2^2 \geq \sum_{i \in S} (\beta + y_i)^2 = \beta^2 |S| + 2\beta \sum_{i \in S} y_i + \sum_{i \in S} y_i^2.$$

Since  $y \geq 0$ , we have  $\sum_{i \in S} y_i = \|y\|_1 \geq \|y\|_2 = t$ , and also  $|S| \geq 1$ . Therefore

$$\|e\|_2^2 \geq \beta^2 + 2\beta t + t^2 = (t + \beta)^2,$$

so  $\|e\|_2 \geq t + \beta$ . Under  $\|e\|_2 \leq R$  this yields  $t \leq R - \beta$ , i.e.,  $\|(e - \beta \mathbf{1})_+\|_2 \leq (R - \beta)_+$ .

Equality holds by taking

$$\begin{aligned} R \leq \beta &: e = 0, \\ R > \beta &: e = R\delta_1. \end{aligned}$$

**Case 2:**  $\beta < 0$ . Write  $\beta = -c$  with  $c > 0$ . Then for any  $e$ ,

$$\|(e - \beta \mathbf{1})_+\|_2 = \|(e + c\mathbf{1})_+\|_2 \leq \|e + c\mathbf{1}\|_2 \leq \|e\|_2 + c\|\mathbf{1}\|_2 \leq R + c\sqrt{m} = R - \beta\sqrt{m}.$$

Equality holds for  $e = \frac{R}{\sqrt{m}}\mathbf{1}$ .  $\square$

### General bias vector

**Theorem A.7** (Worst-case bound for general bias). *Let  $b \in \mathbb{R}^m$  and  $R \geq 0$ . Then*

$$\sup_{\|e\|_2 \leq R} \|(e - b)_+\|_2 = \begin{cases} \max_{i \in [m]} (R - b_i)_+, & b \geq 0 \text{ componentwise,} \\ R + \|b\|_2, & b < 0 \text{ componentwise.} \end{cases}$$

*Proof.*

**Case 1:**  $b < 0$ .

$$\|(e - b)_+\|_2 \leq \|e - b\|_2 \leq R + \|b\|_2.$$

Tightness:  $e = \frac{R}{\|b\|_2}(-b)$  gives exactly  $R + \|b\|_2$ .

**Case 2:**  $b \geq 0$ . For  $i^* = \arg \min_i b_i$ , let  $b_c = b_{i^*} \mathbf{1}$ . Then  $(e - b)_+ \leq (e - b_c)_+$  componentwise, so

$$\|(e - b)_+\|_2 \leq \|(e - b_c)_+\|_2 \stackrel{(A.6)}{\leq} (R - b_{i^*})_+ = \max_i (R - b_i)_+.$$

Tightness:  $e = R\delta_{i^*}$  for  $i^* = \arg \max_i (R - b_i)_+$  achieves equality.  $\square$

*Remark A.8.* Theorem A.7 identifies two regimes in which the worst-case residual can be characterized exactly: a fully negative bias, where the bound grows linearly with  $\|b_-\|_2$ , and a fully nonnegative bias, where the optimum concentrates on a single coordinate.

**Corollary A.9** (Main deterministic bound). *Let  $b \in \mathbb{R}^m$  and  $R \geq 0$  be such that  $\|\Delta W x\|_2 \leq R$ . Then for all  $x \in \mathbb{R}^d$ ,*

$$\mathcal{E}_b(x) = \frac{\|A(x) - B_b(x)\|_2}{\|x\|_2} \leq \begin{cases} \frac{\max_{i \in [m]} (R - b_i)_+}{\|x\|_2}, & b \geq 0 \text{ componentwise,} \\ \frac{R + \|b\|_2}{\|x\|_2}, & b < 0 \text{ componentwise.} \end{cases}$$

**Corollary A.10** (Truncated SVD). *By Eckart–Young–Mirsky, if  $W_r$  is the rank- $r$  truncated SVD of  $W^{\text{gate}}$ , then  $\|\Delta W\|_2 = \sigma_{r+1}(W^{\text{gate}}) = \sigma_{r+1}$ , so for all  $x \in \mathbb{R}^d$ ,*

$$\mathcal{E}_b(x) \leq \begin{cases} \max_{i \in [m]} \left( \sigma_{r+1} - \frac{b_i}{\|x\|_2} \right)_+, & b \geq 0 \text{ componentwise,} \\ \sigma_{r+1} + \frac{\|b\|_2}{\|x\|_2}, & b < 0 \text{ componentwise.} \end{cases}$$

*Remark A.11.* While rather loose in practice due to data distribution, this bound cleanly separates approximation error  $\sigma_{r+1}$  from gating bias  $b$ , revealing bias addition's influence on residuals.

## A.2. Greedy threshold selection

**Greedy threshold calibration under a fixed sparsity budget** We study a data-dependent calibration rule for component-wise thresholds  $\tau \in \mathbb{R}^m$  under a fixed *drop budget*  $K$  (equivalently, fixed sparsity). Throughout, the gate is

$$g_\tau(x) = \mathbf{1}[ABx > \tau],$$

where  $AB$  denotes any rank- $r$  approximation of  $W^{\text{gate}} \in \mathbb{R}^{m \times d}$ ; the specific choice used in our experiments is given in Section 4.1.1.

**Proxy scores and damage weights** Let  $\mathcal{D} = \{x^{(t)}\}_{t=1}^T$  be a dataset and write  $[m] = \{1, \dots, m\}$ ,  $[T] = \{1, \dots, T\}$ . For each coordinate  $i \in [m]$  and sample  $t \in [T]$  define the proxy score

$$s_i^{(t)} := (ABx^{(t)})_i,$$

and define the *marginal damage weight*

$$w_i^{(t)} := \left| \text{ReLU} \left( W_{i,:}^{\text{gate}} x^{(t)} \right) \cdot W_{i,:}^{\text{up}} x^{(t)} \right|^2 \|W_{:,i}^{\text{down}}\|_2^2 \quad (\geq 0). \quad (13)$$

Given thresholds  $\tau$ , the empirical output error incurred by dropping  $(i, t)$  whenever  $s_i^{(t)} \leq \tau_i$  is

$$\mathcal{L}(\tau) = \sum_{t=1}^T \sum_{i=1}^m w_i^{(t)} \mathbf{1}[s_i^{(t)} \leq \tau_i]. \quad (14)$$

*Remark A.12* (Origin of the weight (13)). Consider the standard gated FFN decomposition

$$z(x) = \text{ReLU}(W^{\text{gate}}x) \odot (W^{\text{up}}x), \quad h(x) = W^{\text{down}}z(x).$$

Then  $h(x)$  decomposes into rank-one terms:

$$h(x) = \sum_{i=1}^m z_i(x) W_{:,i}^{\text{down}}, \quad z_i(x) = \text{ReLU}(W_{i,:}^{\text{gate}}x) \cdot W_{i,:}^{\text{up}}x.$$

Dropping the  $i$ -th hidden coordinate removes exactly the contribution  $v_i(x) = z_i(x)W_{:,i}^{\text{down}}$ , hence

$$\|v_i(x)\|_2^2 = \left| \text{ReLU} \left( W_{i,:}^{\text{gate}}x \right) \cdot W_{i,:}^{\text{up}}x \right|^2 \|W_{:,i}^{\text{down}}\|_2^2,$$

which matches (13) for  $x = x^{(t)}$ .

**Prefix formulation and fixed drop budget** Fix  $i \in [m]$ . Sort samples in nondecreasing order of proxy scores:

$$s_{i,(1)} \leq s_{i,(2)} \leq \dots \leq s_{i,(T)},$$

and let  $w_{i,(j)}$  denote the corresponding permuted weights. Define

$$C_i(k) := \sum_{j=1}^k w_{i,(j)}, \quad C_i(0) = 0, \quad \Delta_i(k) := C_i(k) - C_i(k-1) = w_{i,(k)}.$$

For each coordinate  $i$ , setting  $\tau_i$  so exactly  $k_i$  samples satisfy  $s_i^{(t)} \leq \tau_i$  incurs cost  $C_i(k_i)$ . The total loss is thus

$$\mathcal{L}(\tau) = \sum_{i=1}^m C_i(k_i), \quad k_i := \#\{t : s_i^{(t)} \leq \tau_i\} \in \{0, \dots, T\}.$$

With fixed drop budget  $K \in \{0, 1, \dots, mT\}$ , threshold selection reduces to

$$\min_{\substack{k_i \in \{0, \dots, T\} \\ \sum_{i=1}^m k_i = K}} \sum_{i=1}^m C_i(k_i). \quad (15)$$

### Greedy optimality

**Definition A.13** (Global optimality). A feasible solution  $k^* = (k_1^*, \dots, k_m^*)$  with  $\sum_i k_i^* = K$  is *globally optimal* for (15) if

$$\sum_{i=1}^m C_i(k_i^*) \leq \sum_{i=1}^m C_i(k_i) \quad \text{for all feasible } k = (k_1, \dots, k_m).$$

**Assumption A.14** (Monotone marginals within each coordinate). For every  $i \in [m]$ , the marginal increments are nondecreasing:

$$\Delta_i(1) \leq \Delta_i(2) \leq \dots \leq \Delta_i(T).$$

**Theorem A.15** (Greedy is globally optimal). *Initialize  $k_i = 0$  for all  $i$ . For  $\ell = 1, 2, \dots, K$  (drop budget) choose*

$$i_\ell \in \arg \min_{i: k_i < T} \Delta_i(k_i + 1), \quad \text{and update} \quad k_{i_\ell} \leftarrow k_{i_\ell} + 1.$$

*Under Theorem A.14 the resulting  $k$  is globally optimal for (15).*

*Moreover, it can be realized by thresholds  $\tau$  via*

$$\tau_i \in [s_{i,(k_i)}, s_{i,(k_i+1)}],$$

*with conventions  $s_{i,(0)} := -\infty$  and  $s_{i,(T+1)} := +\infty$ .*

*Proof.* The problem is equivalent to selecting exactly  $K$  increments  $\Delta_i(j)$  while respecting prefix constraints: selecting  $\Delta_i(j)$  requires all  $\Delta_i(1), \dots, \Delta_i(j-1)$ .

The greedy algorithm selects the smallest available “next increment”  $\Delta_i(k_i + 1)$  at each step. Let  $G$  be greedy’s sequence of  $K$  increments, and  $O$  any optimal sequence.

Suppose  $G \neq O$ . Let  $a = \Delta_p(k_p + 1)$  be the first (chronologically) greedy increment not in  $O$ . Since  $|G| = |O| = K$ , there exists  $b = \Delta_q(j) \in O \setminus G$ .

Choose  $b$  as the *last* increment of coordinate  $q$  in  $O$  (maximal  $j$ ). Removing  $b$  preserves  $q$ ’s prefix constraint. Adding  $a$  extends  $p$ ’s prefix, also preserving feasibility.

By greedy choice,  $a \leq \Delta_q(k_q + 1)$  where  $k_q$  counts greedy’s selections in  $q$  up to that point. Since  $b \notin G$  but  $O$  includes it,  $j \geq k_q + 1$ . By Theorem A.14 (nondecreasing increments),  $\Delta_q(k_q + 1) \leq \Delta_q(j) = b$ .

Thus  $a \leq b$ , so swapping  $b \leftrightarrow a$  preserves feasibility and does not increase cost. Repeating such exchanges transforms  $O$  into  $G$ , proving optimality.

The threshold realization follows from the definition of  $k_i$ . □

**Remark A.16** (Role of rank- $r$  approximation and empirical validation). Theorem A.15 requires monotone marginal increments after sorting by proxy scores (Theorem A.14). This is *not guaranteed*, since proxy scores  $s_i^{(t)} = (ABx^{(t)})_i$  depend only on rank- $r$  approximation  $AB \approx W^{\text{gate}}$ , while damage, defined above, also involves  $W^{\text{up}}$  and  $W^{\text{down}}$ .

If  $AB$  approximates  $W^{\text{gate}}$  well *on the input data distribution*, then  $(ABx)_i \approx (W^{\text{gate}}x)_i$ , so proxy sorting should align with true damage ordering. In practice, we perform greedy selection over non-overlapping  $\eta$ -step sums to mitigate data noise:

$$S_i^{(m)} := \sum_{j=(m-1)\eta+1}^{m\eta} w_{i,(j)}, \quad m = 1, \dots, \lfloor T/\eta \rfloor.$$

We validate their monotonicity using normalized Kendall tau distance between group sums and their position indices:

$$\tau_i^K := 1 - \frac{K_d(\{S_i^{(m)}\}_{m=1}^M, \{m\}_{m=1}^M)}{M(M-1)},$$

where  $K_d(\tau_1, \tau_2) = \#\{(m_1, m_2) : m_1 < m_2, [\tau_1(m_1) \leq \tau_1(m_2) \wedge \tau_2(m_1) \geq \tau_2(m_2)]\}$  counts discordant pairs.

The use of Kendall tau distance is justified by the fact that it directly quantifies *ordinal consistency* required by Theorem A.14: for all  $m_1 < m_2$ , we expect  $S_i^{(m_1)} \leq S_i^{(m_2)}$ . Formally,  $\tau_i^K$  measures the fraction of concordant pairs while properly accounting for ties – the precise condition for greedy optimality in Theorem A.15. On sample data used to calibrate biases, Figure 6 shows stable Kendall  $\tau_i^K$  in  $[0.9, 1]$ , confirming proxy sorting  $ABx \approx W^{\text{gate}}x$  and the suitability of our greedy approach.

**Remark A.17** (Knapsack reformulation and practical optimality). Problem (15) is a 0–1 knapsack problem with  $mT$  items  $\{\Delta_i(j)\}_{i=1}^m \}_{j=1}^T$ , capacity  $K$ , and prefix constraints that selection of  $\Delta_i(j)$  requires prior selection of  $\Delta_i(1), \dots, \Delta_i(j-1)$ . While standard dynamic programming requires  $O(mTK)$  time, our greedy algorithm runs in  $O((K+m) \log m)$  via priority queue and is *exactly optimal* under Theorem A.14, yielding superior efficiency.

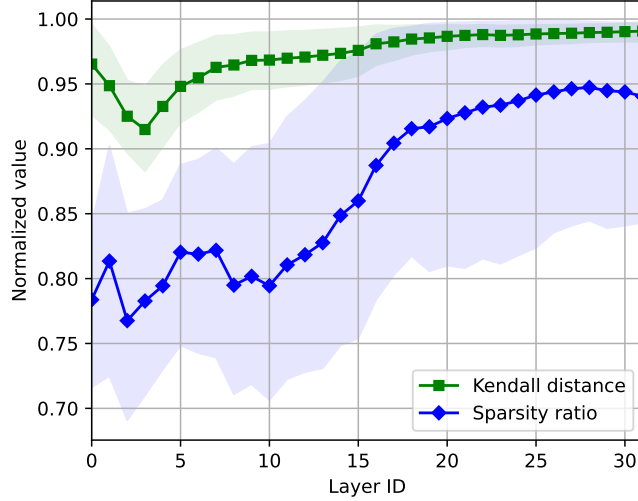


Figure 6. Mean Kendall  $\tau_i^K$  across neurons for proxy-sorted  $\eta$ -step sums from ProSparse-LLaMA2-7B. The x-axis shows layer number. For clarity, layer-wise sparsity ratios are depicted. The shaded regions denote the 10th to 90th percentile interval, illustrating the central 80% of the data distribution.

**Algorithm 3** Sparse FFN Forward Pass on CUDA (Decoding Phase)

```

Input:  $W^{\text{gate}}, W^{\text{up}} \in \mathbb{R}^{D \times d}, W^{\text{down}} \in \mathbb{R}^{d \times D}, x \in \mathbb{R}^d, A \in \mathbb{R}^{D \times r}, B \in \mathbb{R}^{r \times d}, b \in \mathbb{R}^D$ 
Output:  $x \in \mathbb{R}^d$ 
 $m \leftarrow ABx + b$  (Predict sparsity pattern)
 $m \leftarrow \text{SPARSEGATEKERNEL}(W^{\text{gate}}, x, m)$ 
 $x \leftarrow \text{SPARSEUPANDMULKERNEL}(W^{\text{up}}, x, m)$ 
 $x \leftarrow \text{SPARSEDOWNKERNEL}(W^{\text{down}}, x)$ 
return  $x$ 

```

**B. Sparse FFN Inference Implementation**

Unlike DeJa Vu’s (Liu et al., 2023) asynchronous pipeline, which leverages Ampere’s `cuda::memcpy_async` operations (NVIDIA Corporation, 2024), our approach targets consumer-grade GPUs with compute capability 7.0 for broader applicability. Predictors are inserted at the beginning of each FFN and sequentially generate sparsity patterns for their respective gate projections. This design ensures minimal integration overhead with existing frameworks.

**Custom CUDA Kernels for Sparse FFN** We implement three CUDA kernels (Algorithm 3). The predictor’s output  $m \in \mathbb{R}^D$  highlights active rows of  $W^{\text{gate}}$ . Throughout gate and up projections each CUDA block processes one neuron, first verifying its activity via  $m$ . Gate outputs are stored back into  $m$  for reuse. Key optimizations:

- **Memory:** Column-major storage of  $W^{\text{down}}$  for coalesced memory access.
- **Precision:** Full precision register operations; half precision for memory reads and writes.
- **Determinism:** Avoid atomic additions via shared-memory partial sums in down projection.

Our kernel design diverges from existing ProSparse (Song et al., 2024a) and DeJa Vu (Liu et al., 2023) implementations. Both prior approaches rely on atomic addition operations within the down projection phase, introducing non-determinism and potential precision instability during floating-point accumulation. To address these limitations, our algorithm employs partial sum reduction implemented via shared memory. This technique enforces a predefined summation order and utilizes a hierarchical reduction strategy. Consequently, our approach guarantees deterministic outputs while simultaneously achieving enhanced numerical stability through reduced computational error propagation. We postpone kernel fusion due to diminishing returns, prioritizing maintainability.

**Algorithm 4** Sparse FFN Forward Pass on CANN (Decoding Phase)

```

Input:  $W^{\text{gate}}, W^{\text{up}} \in \mathbb{R}^{D \times d}, W^{\text{down}} \in \mathbb{R}^{d \times D}, x \in \mathbb{R}^d, A \in \mathbb{R}^{D \times r}, B \in \mathbb{R}^{r \times d}, b \in \mathbb{R}^D$ 
Output:  $x \in \mathbb{R}^d$ 
 $m \leftarrow ABx + b > 0$  (Predict sparsity pattern)
 $p \leftarrow \text{NONZERO}(m)$  (Obtain indices)
 $g \leftarrow \text{SELROWS}(W^{\text{gate}}, p)$  (Select rows of  $W^{\text{gate}}$  indexed by  $p$ )
 $m_1 \leftarrow \text{MATMUL}(g, x)$ 
 $u \leftarrow \text{SELROWS}(W^{\text{up}}, p)$  (Select rows of  $W^{\text{up}}$  indexed by  $p$ )
 $m_2 \leftarrow \text{MATMUL}(u, x)$ 
 $m_3 \leftarrow \text{RELU}(m_1) \cdot m_2$ 
 $d \leftarrow \text{SELCOLS}(W^{\text{down}}, p)$  (Select columns of  $W^{\text{down}}$  indexed by  $p$ )
 $x \leftarrow \text{MATMUL}(d, m_3)$ 
return  $x$ 

```

**NPU Solution for Sparse FFN** We implement our NPU solution for sparse FFN, detailed in Algorithm 4, leveraging high-level PyTorch instructions. The predictor’s output  $m \in \mathbb{R}^D$  is used to construct smaller dense submatrices by retrieving the corresponding rows or columns. This approach enables highly efficient execution by utilizing the dedicated matrix multiplication accelerator unit (cube) inherent to the CANN NPU architecture (Liao et al., 2019).  $W^{\text{down}}$  matrix is stored in column-major format.

**C. Extension to Non-ReLU Activations**

The solution can in principle be applied to LLMs with non-ReLU activation functions, such as SiLU. However, the straightforward utilization may lead to substantial accuracy degradation on long generation tasks. The quality evaluation results for Qwen2-7B-Instruct model with SiLU activation function are presented at Table 5. Potential modifications to the current solution may include transformations to the intermediate activations to mitigate errors that arise.

Table 5. Qwen2-7B-Instruct accuracy results, 25% average predicted sparsity

Method	TriviaQA acc, %	ARC-C acc, %	ARC-E acc, %	Humaneval pass@1, %	MBPP pass@1, %	GSM8K acc, %	BBH acc, %	CMMLU acc, %	Average
Dense mode	60.96	86.43	93.81	60.98	44.46	36.85	47.81	79.58	63.86
SVDP	51.48	86.43	93.81	49.39	36.55	37.83	47.61	79.58	60.34

**D. Detailed accuracy results**

Table 6, Table 7, Table 8 provide detailed evaluation results for three sparse LLMs equipped with our SVD-predictors. Table 9, Table 11, Table 10 provide a detailed ablation study of SVD sparsity estimators for three sparse LLMs.

Table 6. ProSparse-LLaMA2-7B evaluation results,  $r = 256$

Method	$s$	TriviaQA acc, %	ARC-E acc, %	ARC-C acc, %	Humaneval pass@1, %	MBPP pass@1, %	GSM8K acc, %	BBH acc, %	CMMLU acc, %	Average Score	E2E Speedup
Dense mode	-	62.94	75.42	53.58	17.68	22.59	11.45	35.85	31.84	38.92	1.00×
SVDP	0.4	62.38	75.29	53.67	17.68	22.38	10.61	35.46	31.81	38.66	1.61×
	0.5	62.74	75.34	53.67	17.68	22.07	11.22	35.58	31.94	38.78	1.64×
	0.6	62.90	75.29	53.75	18.29	21.97	10.54	35.54	31.91	38.77	1.67×
	0.7	62.04	75.42	53.58	17.07	21.87	11.22	35.43	31.90	38.57	1.71×

## SVD Contextual Sparsity Predictors for Fast LLM Inference

Table 7. TurboSparse-Mistral-Instruct evaluation results,  $r = 352$

Method	$s$	TriviaQA acc, %	ARC-E acc, %	ARC-C acc, %	Humaneval pass@1, %	MBPP pass@1, %	GSM8K acc, %	BBH acc, %	CMMLU acc, %	Average Score	E2E Speedup
Dense mode	-	48.58	87.21	71.67	34.15	42.20	61.71	42.35	46.52	54.30	1.00×
SVDP	0.4	45.46	87.08	71.67	32.93	42.09	61.49	42.46	46.55	53.72	1.67×
	0.5	43.26	87.04	71.76	33.54	42.71	61.41	42.32	46.47	53.56	1.73×
	0.6	40.63	87.08	72.10	33.54	42.09	61.41	42.19	46.43	53.18	1.79×
	0.7	39.21	87.21	72.10	37.20	42.09	60.96	42.33	46.45	53.44	1.84×

Table 8. SparseQwen2-7B evaluation results,  $r = 512$

Method	$s$	TriviaQA acc, %	ARC-E acc, %	ARC-C acc, %	Humaneval pass@1, %	MBPP pass@1, %	GSM8K acc, %	BBH acc, %	CMMLU acc, %	Average Score	E2E Speedup
Dense mode	-	50.76	91.92	83.87	64.02	46.3	77.1	48.42	64.35	65.84	1.00×
SVDP	0.4	50.87	91.92	83.87	62.80	44.56	76.50	48.40	64.35	65.41	1.78×
	0.5	49.96	91.92	83.87	62.80	43.53	76.80	48.40	64.35	65.20	1.81×
	0.6	48.82	91.92	83.87	63.41	43.53	76.80	48.34	64.35	65.13	1.85×
	0.7	47.42	91.92	83.87	62.20	41.99	75.82	48.36	64.35	64.49	1.86×

## E. Technical details

### E.1. LLMs hyperparameter values

We provide hyperparameter values for the tested models in Table 12, as they influence E2E latency. Specifically, all evaluated optimization techniques modify only the FFN portion of inference, leaving the attention block unchanged. Thus, a higher intermediate size increases the FFN’s contribution to E2E latency. Similarly, the use of Grouped Query Attention reduces the attention contribution to total inference time.

### E.2. Predictor Building

For calibration in total we use 112 few-shot samples ( $\approx 20000$  tokens) from the train splits of the GSM8K, ARC-E, ARC-C, OpenBookQA, QAsper, CodeXGLUE datasets.

### E.3. Predictor’s rank

One can trade off between the predicted sparsity ratio and predictor size. While a larger predictor allows for more sparse computations within gate projection, it requires more compute for prediction. In turn, the  $s$  hyperparameter can be used to calibrate the predicted sparsity ratio. Figure 7 shows how the separation capability of SVD predictors depends on their size. Due to this insight, higher acceleration can be achieved with relatively small predictors. Moreover, small predictors consume less additional memory. Similarly to  $r$ , we set  $s$  to be constant across all layers. Empirically, we found that setting the rank to approximately 2% of the intermediate size  $D$  works well.

SVD Contextual Sparsity Predictors for Fast LLM Inference

Table 9. SVD sparsity estimator ablation study for ProSparseLLAMA2-7B.

	TriviaQA	ARC-E	ARC-C	Humaneval	MBPP	GSM8K	BBH	CMMLU	Average
Dense baseline	62.94	75.42	53.58	17.68	22.59	11.45	35.85	31.84	38.92
<i>Parallel pipeline</i>									
Naive SVD	58.19	69.91	49.32	10.98	13.35	6.60	33.98	30.28	34.08
+ Data whitening	53.85	75.34	53.75	16.46	19.92	10.16	35.46	31.83	37.10
+ Bias calibration	62.66	75.38	53.58	17.68	22.18	10.54	35.86	31.85	38.72
<i>Sequential pipeline</i>									
Naive SVD	34.53	3.58	4.35	0.61	0.21	1.90	11.12	21.23	9.69
+ Data whitening	27.58	75.21	53.33	8.54	11.40	6.90	33.71	31.34	31.00
+ Bias calibration	62.74	75.34	53.67	17.68	22.07	11.22	35.58	31.94	38.78

Table 10. SVD sparsity estimator ablation study for SparseQwen2-7B.

	TriviaQA	ARC-E	ARC-C	Humaneval	MBPP	GSM8K	BBH	CMMLU	Average
Dense baseline	50.76	91.92	83.87	64.02	46.30	77.10	48.42	64.35	65.84
<i>Parallel pipeline</i>									
Naive SVD	46.24	91.92	83.87	53.66	34.39	74.00	48.00	64.35	62.05
+ Data whitening	42.92	91.92	83.87	61.59	43.02	75.89	48.37	64.35	63.99
+ Bias calibration	50.20	91.92	83.87	62.20	45.28	76.65	48.45	64.35	65.37
<i>Sequential pipeline</i>									
Naive SVD	40.03	91.92	83.87	12.20	9.03	63.00	48.43	64.35	51.60
+ Data whitening	30.00	91.92	83.87	57.32	37.78	72.93	48.22	64.35	60.80
+ Bias calibration	49.96	91.92	83.87	62.80	43.63	76.80	48.40	64.35	65.22

Table 11. SVD sparsity estimator ablation study for TurboSparse-Mistral-Instruct.

	TriviaQA	ARC-E	ARC-C	Humaneval	MBPP	GSM8K	BBH	CMMLU	Average
Dense baseline	48.58	87.21	71.67	34.15	42.20	61.71	42.35	46.52	54.30
<i>Parallel pipeline</i>									
Naive SVD	41.40	87.04	71.76	24.39	38.91	60.20	42.13	46.34	51.52
+ Data whitening	37.98	86.57	71.25	37.20	41.79	60.88	42.27	46.18	53.02
+ Bias calibration	46.21	87.12	71.76	36.59	41.89	62.24	42.44	46.45	54.34
<i>Sequential pipeline</i>									
Naive SVD	35.29	71.09	57.85	1.83	8.73	9.17	37.72	25.24	30.87
+ Data whitening	18.09	87.12	72.27	29.27	28.44	48.60	41.87	46.22	46.49
+ Bias calibration	43.26	87.04	71.76	33.54	42.71	61.41	42.32	46.47	53.56

Table 12. LLMs hyperparameter values.

Model	hyperparameters			
	hidden size	intermediate size	n attention heads	n KV heads
ProSparse-LLaMA2-7B	4096	11008	32	32
TurboSparse-Mistral-Instruct	4096	14336	32	8
SparseQwen2-7B	3584	18944	28	4

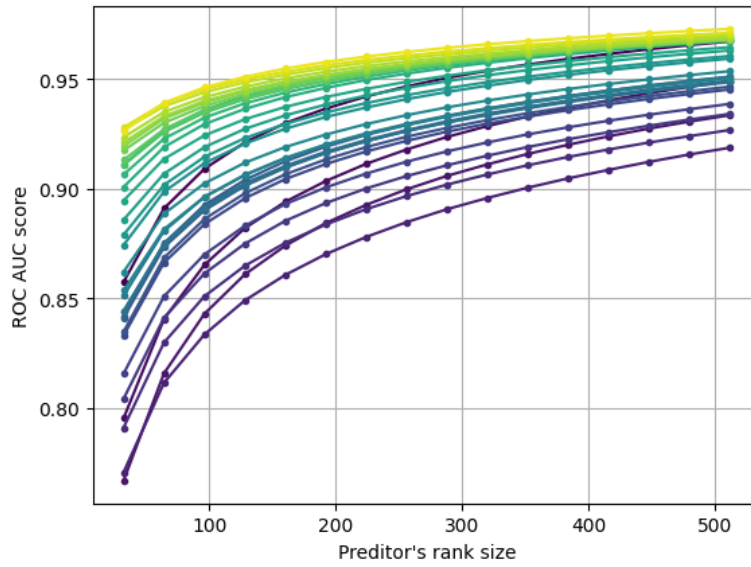


Figure 7. ROC AUC scores of SVD-predictors at different layers averaged across several sequence samples for ProSparse-LLaMA2-7B. The brighter curves represent deeper layers. For most of the layers a quality metric reaches a plateau at relatively small rank.